2022 IEEE Intelligent Vehicles Symposium (IV)
June 5-9, 2022. Aachen, Germany

Multi-vehicle Conflict Management with Status and Intent Sharing

Hao M. Wang, Sergei S. Avedisov, Onur Altintas, and Gábor Orosz

***Abstract*— In this paper, we extend the conflict analysis framework to resolve conflicts between multiple vehicles with different levels of automation, while utilizing status-sharing and intent-sharing enabled by vehicle-to-everything (V2X) communication. In status-sharing a connected vehicle shares its current state (e.g., position, velocity) with other connected vehicles, whereas in intent-sharing a vehicle shares information about its future trajectory (e.g., velocity bounds). Our conflict analysis framework uses reachability theory to interpret the information contained in status-sharing and intent-sharing messages through conflict charts. These charts enable real-time decision making and control of a connected automated vehicle interacting with multiple remote connected vehicles. Using numerical simulations and real highway traffic data, we demonstrate the effectiveness of the proposed conflict resolution strategies, and reveal the benefits of intent sharing in mixed-autonomy environments.**

2022 IEEE Intelligent Vehicles Symposium (IV) | 978-1-6654-8821-1/22/$31.00 ©2022 IEEE | DOI: 10.1109/IV51971.2022.9827428

I. Introduction

Road participants may be involved in conflicts during cooperative maneuvering if their trajectories intersect or come sufficiently close. Such conflicts must be detected and resolved in a timely manner to ensure the safety and efficiency of traffic. Earlier results show that in a fully automated environment, vehicle-to-everything (V2X) communication can enable vehicles to negotiate and agree on future maneuvers, and conflicts can be managed in a cooperative way by a variety of control techniques [1]–[4].

In the next few decades, one can expect mixed-autonomy environments where vehicles of different automation levels [5] and cooperation classes [1] share the roadways. Recent studies focus on conflict resolution in such scenarios. Methods such as game theory [6], reachability analysis [7], and model predictive control [8] were used for decision making and action planning, while uncertainties in GPS information were considered in [9]. Our previous work [10]–[12] proposed a tool called conflict analysis to prevent conflicts in mixed-autonomy environments. We considered two vehicles using status-sharing cooperation and intent-sharing cooperation via V2X. In status-sharing cooperation connected vehicles transmit their current state, for example, GPS position and velocity by using basic safety messages (BSMs) [13]. In intent-sharing cooperation connected vehicles share information about their future trajectory, for example, velocity bounds or acceleration bounds that will be used in the near future [1]. In this paper, we generalize conflict analysis to scenarios including more than two vehicles, while considering both status- and intent-sharing cooperation.

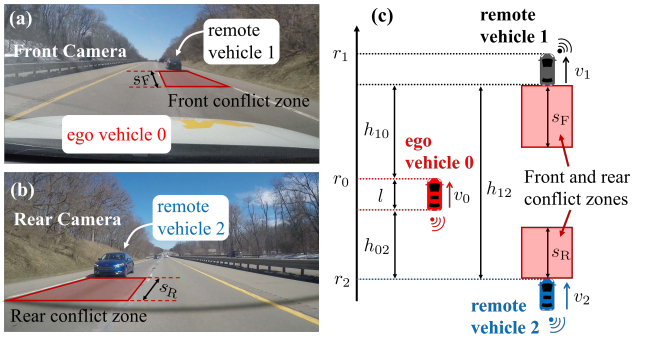

Fig. 1. Cooperative maneuvering involving three vehicles with potential conflict. (a-b) Front and rear camera views from the ego vehicle 0 at the moment when it decides to move into the target lane between remote vehicle 1 and remote vehicle 2; (c) the generalized model where the red-shaded regions highlight the front and rear conflict zones.

Figure 1(a)-(b) depict a maneuver involving potential conflicts where an ego vehicle performs a lane change into the right lane between two remote vehicles on a highway. Such lane change maneuvers consist of two steps: (i) the ego vehicle forms appropriate front and rear gaps with the remote vehicles while staying in its current lane; (ii) the ego vehicle moves into the target lane by changing its lateral position. Here we focus on step (i) and assume that step (ii) is carried out by lateral motion planners and controllers once a gap is ensured. We define two rectangle-shaped conflict zones to represent the safety buffers between the ego vehicle and two remote vehicles; see the red shaded areas in Fig. 1. These conflict zones are moving together with the corresponding remote vehicles and their sizes may vary according to road configurations. To prevent conflict in a lane change, the ego vehicle must form necessary front and rear gaps such that it does not overlap with the two conflict zones.

We resolve conflicts from the perspective of the ego vehicle and assume that it receives status sharing and intent sharing messages from both remote vehicles. That is, our conflict analysis does not assume any specific functions for the remote vehicles, other than that they are connected vehicles. We propose a reachability-based method to numerically calculate the so-called no-conflict, uncertain, and conflict sets partitioning the state space into different domains in terms of conflict prevention. This allows for efficient and reliable decision making and controller design which guarantees conflict-free maneuvers. We show that with intent information, the performance of ego vehicle can be significantly improved. These benefits are quantified using real highway data.

Hao M. Wang and Gábor Orosz are with the Department of Mechanical Engineering, University of Michigan, Ann Arbor, MI 48109, USA. {haowangm, orosz}@umich.edu.

Sergei S. Avedisov and Onur Altintas are with Toyota Motor North America R&D – InfoTech Labs, Mountain View, CA 94043, USA. {sergei.avedisov, onur.altintas}@toyota.com.

Gábor Orosz is also with the Department of Civil and Environmental Engineering, University of Michigan, Ann Arbor, MI 48109, USA.

II. Modeling Vehicle Dynamics

Consider the scenario in Fig. 1(a-b) where the ego vehicle 0 attempts to move into the target lane in between remote vehicle 1 and remote vehicle 2. As mentioned before, we focus on the first step of the lane change maneuver, where the ego vehicle needs to form necessary longitudinal gaps before crossing the lane markings laterally. The conflict zone lengths s_{F} and s_{R} represent minimal front and rear distances the ego vehicle must secure to ensure a conflict-free lane change. Considering the restricted velocity ranges in typical highway driving scenarios, we consider constant s_{F} and s_{R}; see Table I. This simplification is used to better highlight the main idea of conflict analysis, while the results can be easily adapted to non-constant s_{F} and s_{R}. Fig. 1(c) shows the generalized model where r_0, r_1 and r_2 denote the positions of the vehicles' front bumpers, and v_0, v_1 and v_2 denote their longitudinal velocities. We assume that all vehicles have the same length l.

By neglecting the air and rolling resistances, the longitudinal dynamics of the vehicles can be described by

$$\dot{r}_i(t) = v_i(t), \quad \dot{v}_i(t) = \mathrm{sat}(u_i(t)), \quad i = 0, 1, 2. \tag{1}$$

Here the dot denotes the derivative with respect to time t, and u_0, u_1 and u_2 are the control inputs, and the saturation function $\mathrm{sat}(\cdot)$ represents the acceleration limits. When $v \in (v_{\min}, v_{\max})$, we have

$$\mathrm{sat}(u) = \max\big\{\min\{u, a_{\max}\}, a_{\min}\big\}. \tag{2}$$

For $v = v_{\min}$, we substitute $a_{\min}$ with 0, since the vehicle would not decelerate; for $v = v_{\max}$, we substitute $a_{\max}$ with 0, since the vehicle would not accelerate. All parameter values used in this paper are summarized in Table I, which correspond to typical highway driving scenarios. We assume that these limits are known to the ego vehicle.

The positions r_1, r_2 and velocities v_1, v_2 of the remote vehicles are made available to the ego vehicle via V2X communication, and these are used in decision making and in determining the control input u_0. We consider that the remote vehicles can use messages pertaining to two classes of cooperation: status sharing and intent sharing. We assume that messages from both remote vehicles are received by the ego vehicle in a synchronized manner, and we define the initial time as the time when the first pair of status packets are received. When intent-sharing messages are available from the remote vehicles, the ego vehicle may use those to achieve a better prediction of its future environment. Note that we do not have control over the remote vehicles' motion, i.e., we cannot prescribe inputs u_1 and u_2.

Below we define the relative distances between vehicles:

$$h_{10} := r_1 - r_0 - l, \quad h_{02} := r_0 - r_2 - l, \quad h_{12} := r_1 - r_2 - l, \tag{3}$$

where h_{10} and h_{02} are the front and rear gaps between the ego vehicle 0 and remote vehicles 1 and 2, respectively, and h_{12} is the total gap between the two remote vehicles; see Fig. 1(c). Note that these gaps are signed bumper to bumper distances. Also note that $h_{12} = h_{10} + h_{02} + l \geq 0$ because the remote vehicle 2 is assumed to travel behind vehicle 1. This leads to $h_{10} + h_{02} \geq -l$. Since relative distances (3) play a key role in lane change maneuvers, we define the state of the system (1) as

$$\mathbf{x} := [h_{10}, h_{02}, v_0, v_1, v_2]^\top \in \Omega, \tag{4}$$

where the domain Ω is given by

$$\begin{aligned}\Omega := &\{[h_{10}, h_{02}]^\top \in \mathbb{R}^2 | h_{10} + h_{02} \geq -l\} \times [v_{\min,0}, v_{\max,0}] \\ &\times [v_{\min,1}, v_{\max,1}] \times [v_{\min,2}, v_{\max,2}].\end{aligned} \tag{5}$$

III. Conflict Analysis

In this section, we use formal logic to provide a rigorous description of conflict. Then we propose a reachability analysis-based method to calculate the sets partitioning the state space into domains with different qualitative behaviors with respect to conflict prevention.

As mentioned above, before changing lanes, the ego vehicle must secure necessary front and rear gaps with respect to the remote vehicles 1 and 2. Such a conflict-free maneuver can be formally described by the proposition

$$P := \{\exists t \geq 0, h_{10}(t) \geq s_{\mathrm{F}} \wedge h_{02}(t) \geq s_{\mathrm{R}}\}, \tag{6}$$

where the symbol $\wedge$ (and) is used. Proposition P can be further decomposed into three cases:

(i) No-conflict case: ego vehicle 0 is able to prevent conflict independent of the motion of remote vehicles 1 and 2.
(ii) Uncertain case: ego vehicle 0 may be able to prevent conflict depending on the motion of remote vehicles 1 and 2.
(iii) Conflict case: ego vehicle 0 is not able to prevent conflict independent of the motion of remote vehicles 1 and 2.

These cases correspond to three pairwise disjoint sets in the state space Ω of system (1):

$$\mathcal{P}_{\mathrm{g}} := \{\mathbf{x}(0) \in \Omega | \forall u_1(t), \forall u_2(t), \exists u_0(t), P\}, \tag{7}$$

$$\begin{aligned}\mathcal{P}_{\mathrm{y}} := \{\mathbf{x}(0) \in \Omega | &(\exists u_1(t), \exists u_2(t), \forall u_0(t), \neg P) \wedge \\ &(\exists u_1(t), \exists u_2(t), \exists u_0(t), P)\},\end{aligned} \tag{8}$$

$$\mathcal{P}_{\mathrm{r}} := \{\mathbf{x}(0) \in \Omega | \forall u_1(t), \forall u_2(t), \forall u_0(t), \neg P\}. \tag{9}$$

Here the symbol $\neg$ means negation, and the subscripts g, y, and r correspond to the colors green, yellow, and red used to visualize these domains in the state space, corresponding to the no-conflict, uncertain, and conflict case respectively; see Fig. 2. Since the first and second predicates in (8) are the negations of the predicates in (7) and (9), respectively, we have $\mathcal{P}_{\mathrm{g}} \cup \mathcal{P}_{\mathrm{y}} \cup \mathcal{P}_{\mathrm{r}} = \Omega$.

Figure 2(a) shows these sets in (h_{10}, h_{02})-plane for velocities $(v_0, v_1, v_2) = (27, 29, 28)$ [m/s], where the white region

TABLE I
PARAMETERS VALUES USED IN THE PAPER.

s_{F}, s_{R}	10 [m]	l	5 [m]
$a_{\min,0}$	-8 [m/s^2]	$a_{\min,1}$, $a_{\min,2}$	-4 [m/s^2]
$a_{\max,0}$	4 [m/s^2]	$a_{\max,1}$, $a_{\max,2}$	2 [m/s^2]
$v_{\min,0}$	22 [m/s]	$v_{\min,1}$, $v_{\min,2}$	25 [m/s]
$v_{\max,0}$	38 [m/s]	$v_{\max,1}$, $v_{\max,2}$	35 [m/s]

is outside the state space Ω; cf. (5). We refer to this as a conflict chart. One can reason about conflicts by locating the current vehicle state in this chart. Notice that $\mathcal{P}_{\rm r} = \emptyset$ holds under a reasonable condition of behavior parameters: $v_{\max,1} > v_{\min,2}$, $v_{\max,0} > v_{\min,2}$, and $v_{\min,0} < v_{\max,1}$; see Table I. These conditions allow the remote vehicles to make a large enough total gap (if vehicle 1 accelerates and vehicle 2 slows down), so that the ego vehicle is able to move in eventually without conflict. Thus, in the rest of this section, we focus on $\mathcal{P}_{\rm g}$ and $\mathcal{P}_{\rm y}$.

Below we provide a method to check whether an initial state $\mathbf{x}(0)$ belongs to $\mathcal{P}_{\rm g}$ or $\mathcal{P}_{\rm y}$. The sets can then be obtained using a brute force method, i.e., checking each state in the state space Ω. Note that, however, in practice there is no need to calculate the whole sets $\mathcal{P}_{\rm g}$ and $\mathcal{P}_{\rm y}$. The ego vehicle may simply check which set the state is in using the latest information received from the remote vehicles.

If $h_{10}(0) \geq s_{\rm F} \wedge h_{02}(0) \geq s_{\rm R}$, we have $\mathbf{x}(0) \in \mathcal{P}_{\rm g}$ immediately since the ego vehicle already formed the necessary front and rear gaps at the initial time; otherwise, one needs to check if proposition P is true for some $t > 0$, considering all possible future behaviors of the ego and remote vehicles. The Lemma below demonstrates that when checking $\mathbf{x}(0) \in \mathcal{P}_{\rm g}$, the behavior limits of the remote vehicles need to be used.

Lemma 1: The following relationship holds for any given initial state $\mathbf{x}(0) \in \Omega$:

$$\{\forall u_1(t), \forall u_2(t), \exists u_0(t), P\} \iff \{(u_1(t), u_2(t)) \equiv (a_{\min,1}, a_{\max,2}), \exists u_0(t), \exists t \in T, h_{10}(t) \geq s_{\rm F} \wedge h_{02}(t) \geq s_{\rm R}\}, \tag{10}$$

where $T = \{t \geq 0 | h_{12}(t) \geq s_{\rm F} + s_{\rm R} + l\}$.

Proof: See Appendix I. ∎

Here the set T represents a time interval within which the ego vehicle must form the necessary front and rear gaps to prevent conflicts, under the worst-case behaviors of the remote vehicles (given by their input limits). Thus, checking $\mathbf{x}(0) \in \mathcal{P}_{\rm g}$ is equivalent to examining the existence of an input $u_0(t)$ and a time $t \in T$ such that $h_{10}(t) \geq s_{\rm F} \wedge h_{02}(t) \geq s_{\rm R}$ holds assuming worst-case behaviors of the remote vehicles. The following Theorem provides a reachability-based criterion to do this.

Theorem 1: Given the dynamics (1,2) and the initial state $\mathbf{x}(0) \in \Omega$, $\mathbf{x}(0) \in \mathcal{P}_{\rm g}$ holds if and only if the condition

$$\Gamma := \bigcup_{t \in T} [s_{\rm R}, \delta(t)] \cap \bigcup_{t \in T} \mathcal{R}_{h_{02}}(t) \neq \emptyset, \tag{11}$$

is satisfied under $(u_1(t), u_2(t)) \equiv (a_{\min,1}, a_{\max,2})$, where $\delta(t) = h_{12}(t) - s_{\rm F} - l$, $\mathcal{R}_{h_{02}}(t) = [h_{02}^{\min}(t), h_{02}^{\max}(t)]$, and the analytical forms of $\delta(t)$, $h_{02}^{\min}(t)$, and $h_{02}^{\max}(t)$ are given in Appendix II.

Proof: See Appendix III. ∎

Here the set $\bigcup_{t \in T} [s_{\rm R}, \delta(t)]$ gives the values of the time t and the rear gap h_{02} such that $h_{10}(t) \geq s_{\rm F} \wedge h_{02}(t) \geq s_{\rm R}$ under the worst-case behaviors of remote vehicles, while ignoring the ego vehicle's motion capability to achieve it. On the other hand, the set $\bigcup_{t \in T} \mathcal{R}_{h_{02}}(t)$ contains all rear gap values that the ego vehicle is able to reach (i.e., the projection of the reachable tube of system (1) to (t, h_{02})). Thus, the intersection Γ gives all feasible rear gaps and the corresponding times when the ego vehicle can secure $h_{10}(t) \geq s_{\rm F} \wedge h_{02}(t) \geq s_{\rm R}$. We refer to Γ as the opportunity set and denote the corresponding time window by $T_{\rm w}$. Fig. 2(b) depicts the above sets. Here the black curve is computed assuming $(u_1(t), u_2(t)) \equiv (a_{\min,1}, a_{\max,2})$ while the red and blue curves are computed by assuming $(u_0(t), u_2(t)) \equiv (a_{\max,0}, a_{\max,2})$ and $(u_0(t), u_2(t)) \equiv (a_{\min,0}, a_{\max,2})$, respectively; see [14] for more examples of reachable sets and tubes.

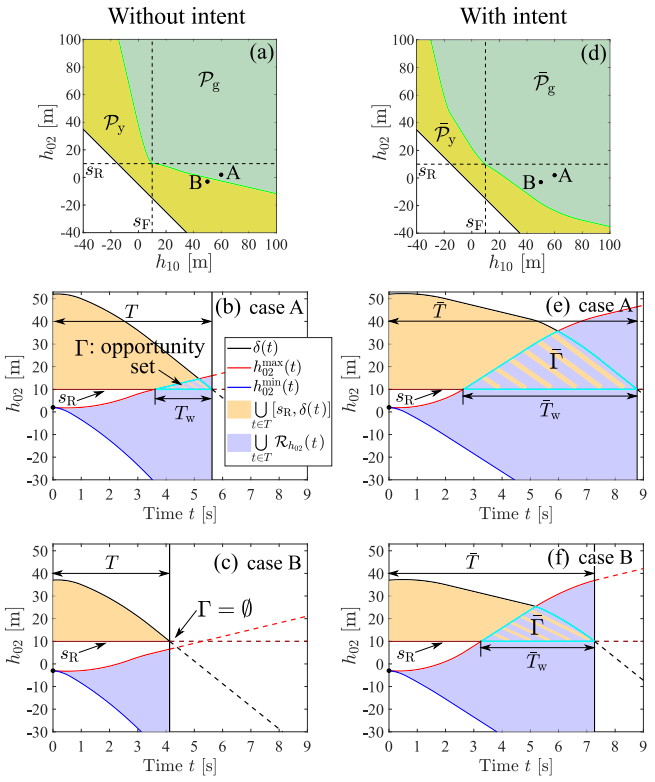

Fig. 2. (a)-(c) Conflict analysis without intent information. (a) Conflict chart in (h_{10}, h_{02})-plane for $(v_0, v_1, v_2) = (27, 29, 28)$ [m/s]. (b)-(c) Mechanisms of checking opportunity set Γ with initial front and rear gaps corresponding to point A at $(h_{10}(0), h_{02}(0)) = (60, 2)$ [m] and point B at $(h_{10}(0), h_{02}(0)) = (50, -3)$ [m]. (d)-(f) Conflict analysis with intent information $v_1(t), v_2(t) \in [27, 30]$ [m/s], $u_1(t), u_2(t) \in [-1, 1]$ [m/s^2], and $\Delta t_1 = \Delta t_2 = 5$ [s].

We emphasize that Theorem 1 reduces the checking of $\mathbf{x}(0) \in \mathcal{P}_{\rm g}$ to the checking of intersection of two sets which are given analytically. This can be done efficiently with numerical methods and is suitable for real time implementation. For more complex dynamics, the set $\mathcal{R}_{h_{02}}(t)$ may not be expressed analytically, and one shall utilize approximation techniques to compute reachable sets [15]. Fig. 2(b) shows the case when $\Gamma \neq \emptyset$ as indicated by the striped region. This corresponds to $\mathbf{x}(0) \in \mathcal{P}_{\rm g}$; see point A in Fig. 2(a). Fig. 2(c) shows the case $\Gamma = \emptyset$. This corresponds to $\mathbf{x}(0) \in \mathcal{P}_{\rm y}$; see point B in Fig. 2(a). If $\mathbf{x}(0) \in \mathcal{P}_{\rm g}$, conflict can be avoided, so the ego vehicle's decision is to change lane. If $\mathbf{x}(0) \in \mathcal{P}_{\rm y}$, it may not be able to change lanes without conflict. Thus, the ego vehicle decides to keep its current lane.

IV. Conflict analysis with intent information

In this section, we show that receiving intent information from remote vehicles can benefit the decision making of the ego vehicle. Intent sharing reduces the conservatism in the prediction of the remote vehicles' future behaviors compared to status sharing. First, we give the formal definition of intent.

Definition 1: Given the dynamics (1,2), the intent of remote vehicle i is a restricted velocity domain $v_i(t) \in [\underline{v}_i, \bar{v}_i]$ and acceleration (input) domain $u_i(t) \in [\underline{a}_i, \bar{a}_i]$ over the time period $t \in [0, \Delta t_i]$, where $v_{\min,i} \le \underline{v}_i \le \bar{v}_i \le v_{\max,i}$ and $a_{\min,i} \le \underline{a}_i \le \bar{a}_i \le a_{\max,i}$. ■

For example, in a highway driving scenario, an intent message may contain the information that for the next $\Delta t_i = 5$ seconds, the remote vehicle i will be traveling with velocity between $\underline{v}_i = 27$ and $\bar{v}_i = 30$ [m/s] while restricting its acceleration between $\underline{a}_1 = -1$ and $\bar{a}_1 = 1$ [m/s^2].

When intent information is available, we denote the no-conflict, uncertain, and conflict sets as $\bar{\mathcal{P}}_{\rm g}$, $\bar{\mathcal{P}}_{\rm y}$, and $\bar{\mathcal{P}}_{\rm r}$ respectively. Lemma 1 and Theorem 1 hold by substituting $(u_1(t), u_2(t)) \equiv (a_{\min,1}, a_{\max,2})$ with

$$u_1(t) = \begin{cases} \underline{a}_1, & \text{if } t \le \Delta t_1, \\ a_{\min,1}, & \text{otherwise,} \end{cases} \quad u_2(t) = \begin{cases} \bar{a}_2, & \text{if } t \le \Delta t_2, \\ a_{\max,2}, & \text{otherwise,} \end{cases} \tag{12}$$

which represents remote vehicles' worst future behaviors under the given intent information. Based on this, one can prove that the following relationships hold:

$$\mathcal{P}_{\rm g} \subseteq \bar{\mathcal{P}}_{\rm g}, \quad \mathcal{P}_{\rm y} \supseteq \bar{\mathcal{P}}_{\rm y}, \quad \mathcal{P}_{\rm r} = \bar{\mathcal{P}}_{\rm r} = \emptyset. \tag{13}$$

That is, intent sharing expands the no-conflict (green) set while shrinking the uncertain (yellow) set; cf. Fig. 2(a) and (d). Note that $\bar{\mathcal{P}}_{\rm g}$ and $\bar{\mathcal{P}}_{\rm y}$ revert to $\mathcal{P}_{\rm g}$ and $\mathcal{P}_{\rm y}$ if no intent is shared. Also, the conflict set (red) remains empty. By superimposing conflict charts Fig.2(a) and (d), the benefit of intent in terms of decision making is quantified in Fig. 3(a). The gray-shaded region is where the decision to make a lane change or not remains unchanged. Part of the previously yellow region now becomes green, and thus, makes the ego vehicle confident enough to pursue the lane change opportunity.

Moreover, by denoting the opportunity set and the corresponding time window as $\bar{\Gamma}$ and $\bar{T}_{\rm w}$ under intent information, one can prove that

$$T_{\rm w} \subseteq \bar{T}_{\rm w}. \tag{14}$$

This suggests that, given the same initial state, with intent information, the ego vehicle becomes aware of a larger opportunity window. This is illustrated in Fig. 2(e)-(f), which correspond to the same initial state as Fig. 2(b)-(c); see points A and B in Fig. 2(a)-(d). Note that for case B, the opportunity set becomes nonempty under intent, as point B is now located inside the expanded green region. Calculation of the opportunity set $\bar{\Gamma}$ can be done similarly as discussed in the previous section; see also Appendix. II.

The heat map plotted in Fig. 3(b) quantifies the additional time window $\Delta T_{\rm w} = |\bar{T}_{\rm w}| - |T_{\rm w}|$ gained due to the intent,

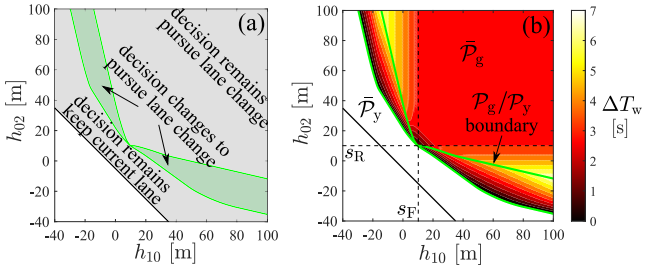

Fig. 3. (a) Change of decision chart under the same intent information and initial velocities as in Fig.2(d)-(f). (b) Heat map of additional time windows $\Delta T_{\rm w} = |\bar{T}_{\rm w}| - |T_{\rm w}|$.

where $|\cdot|$ denotes the lengths of window. The green curves correspond to those in the conflict charts in Fig. 2(a),(d). Regions where time window does not exist with intent sharing are left blank. With intent, the time window increases everywhere in the set $\bar{\mathcal{P}}_{\rm g}$ and large benefits appear near $\mathcal{P}_{\rm g}/\mathcal{P}_{\rm y}$ boundary. The heat map also reveals that even in the domain where the decision to pursue lane change remains unchanged, larger time windows are secured compared to the no-intent case.

V. Controller design and simulation

In this section, we design a controller for the ego vehicle to form necessary longitudinal gaps for a conflict-free lane change. Then we demonstrate the effectiveness of the conflict analysis framework and compare status and intent sharing using simulations with real highway data.

A. Controller design

For $\mathbf{x}(0) \in \mathcal{P}_{\rm g}$, the opportunity set $\Gamma \neq \emptyset$ and each point $(t, h_{02}) \in \Gamma$ gives a feasible rear gap and a corresponding time assuming the worst-case behaviors of the remote vehicles. Note that once this rear gap is formed, the necessary front gap is also guaranteed simultaneously. Thus, the control input $u_0(t)$ can be designed by selecting an appropriate goal point $(t^{\rm G}, h_{02}^{\rm G}) \in \Gamma$. From robustness viewpoint, we select the center point of the opportunity set as the goal, i.e., choose $t^{\rm G}$ in the middle of $T_{\rm w}$ and $h_{02}^{\rm G}$ in the middle of the slice of Γ at $t^{\rm G}$; see the black point in Fig. 4(a). We design a constant value control input $u_0(t) = u_0^{\rm G}$ for the ego vehicle to pursue the goal point $(t^{\rm G}, h_{02}^{\rm G}) \in \Gamma$. The analytical form of $u_0^{\rm G}$ is given in Appendix IV. The gray arrow in Fig. 4(a) depicts the expected trajectory $h_{02}(t)$ under the designed constant input. Note that the domain $\mathcal{P}_{\rm g}$ (or $\bar{\mathcal{P}}_{\rm g}$ if intent is available) is invariant under $u_0^{\rm G}$ independent of remote vehicles' motions.

We remark that once new status and/or intent updates are received from the remote vehicles, the opportunity set Γ is recalculated, and the goal point $(t^{\rm G}, h_{02}^{\rm G}) \in \Gamma$ and the corresponding control input $u_0^{\rm G}$ is also updated. As shown by simulation examples below, frequent status and intent updates benefit the time efficiency and passenger comfort of the ego vehicle.

B. Simulation with real highway data

To represent remote vehicles, we utilize data collected from real human-driven vehicles involved in a lane change

TABLE II

MANEUVER RESULTS UNDER DIFFERENT V2X CONDITIONS.

V2X condition	Maneuver result
Status sharing only	Lane change opportunity missed
Status and intent sharing 1 [s] update rate	Lane change opportunity secured Maneuver time 6.0 [s]
Status and intent sharing 0.1 [s] update rate	Lane change opportunity secured Maneuver time 5.3 [s]

maneuver on highway I-94 near Ann Arbor, Michigan; see Fig. 1(a)-(b). During this maneuver, the remote vehicles were using cruise control and their speed and acceleration data are shown in Fig. 5(a)-(b). We consider the ego vehicle as a connected automated vehicle attempting to change lanes and to move in between the remote vehicles.

At the initial time, the front and rear gaps are 56.62 and -10.14 [m], while the ego vehicle, remote vehicle 1, and remote vehicle 2 are traveling with speeds 33.18, 29.68, and 29.62 [m/s], respectively, i.e., the ego vehicle is traveling behind both remote vehicles. This yields $\mathbf{x}(0) \in \mathcal{P}_{\mathrm{y}}$ and the ego vehicle is not confident enough to perform a lane change with status-sharing information. Thus, if the remote vehicles only share status information, the opportunity to change lanes is missed. However, intent information can significantly improve the decision. We can extract the intent information of the remote vehicles when they run cruise control on a real highway as $v_1(t), v_2(t) \in [29, 30]$ [m/s] and $u_1(t), u_2(t) \in [-0.2, 0.2]$ [m/s^2]. If we assume the intent for both vehicles lasts for $\Delta t_1 = \Delta t_2 = 8$ [s], this yields $\mathbf{x}(0) \in \bar{\mathcal{P}}_{\mathrm{g}}$, that is, the ego vehicle decides to pursue the lane change by using the controller $u_0(t) = u_0^{\mathrm{G}}$.

Figure 4(a)-(d) show the evolution of opportunity set $\bar{\Gamma}$, the goal point $(t^{\mathrm{G}}, h_{02}^{\mathrm{G}}) \in \bar{\Gamma}$, and trajectory $h_{02}(t)$ (green curve), when status and intent are updated every 0.1 [s]. Note that for intent update, the velocity and acceleration bounds remain the same, but the time horizon is extended by the update. At 5.3 [s], the ego vehicle already forms the necessary rear gap (and front gap), and the lane change can be started instead of further chasing the goal point. That is, the goal point serves as a guidance for the ego vehicle's motion until the adequate gaps form, and there is no need to actually reach it. The corresponding time profiles are shown in solid green curves in Fig. 5. If status and intent are updated only every 1 [s], the ego vehicle still decides to go for the lane change but the necessary rear and front gaps only form at 6.0 [s] and the control command becomes less smooth; see dashed green curves in Fig. 5. That is, with frequent status and intent updates, the time efficiency and passenger comfort of the ego vehicle is significantly improved. These results are summarized in Table II.

VI. CONCLUSION

In this paper we constructed the conflict analysis framework for cooperative maneuvers involving multiple vehicles with different automation levels. Specifically, conflict analysis was used to examine the merits of vehicle-to-vehicle communication in preventing conflicts during lane changes.

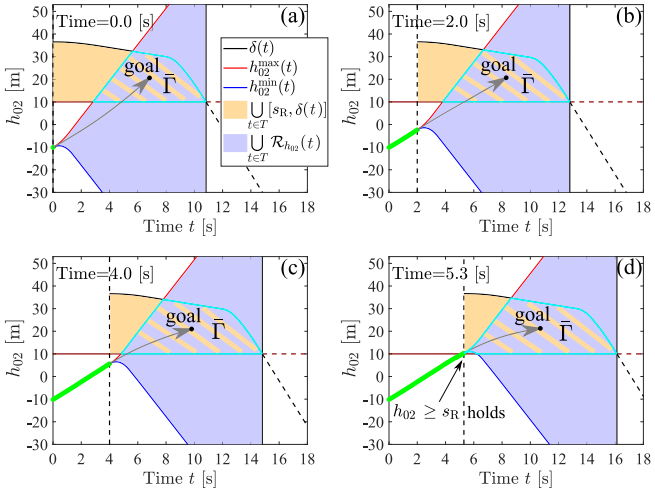

Fig. 4. Evolution of opportunity set $\bar{\Gamma}$, goal point, and trajectory $h_{02}(t)$ with initial state $(h_{10}, h_{02}) = (56.62, -10.14)$ [m], $(v_0, v_1, v_2) = (33.18, 29.68, 29.62)$ [m/s], and intent information $v_1, v_2 \in [29, 30]$ [m/s], $u_1, u_2 \in [-0.2, 0.2]$ [m/s^2], $\Delta t_1 = \Delta t_2 = 8$ [s], using controller $u_0(t) = u_0^{\mathrm{G}}$ with status and intent updates every 0.1 [s].

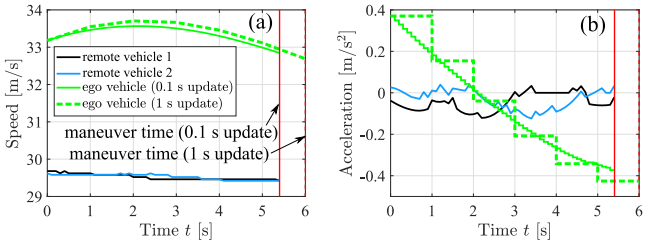

Fig. 5. Simulation results using the same initial state and intent as in Fig. 4 with different status and intent update rates.

We considered status-sharing communication (where connected vehicles share their current states) and intent-sharing communication (where they also share information about their future motion). We demonstrated that receiving status-sharing messages helps a connected automated vehicle to execute conflict-free maneuvers. Moreover, intent-sharing can be used to remove the conservatism from decision making, and improve efficiency of the controllers. The benefits are demonstrated by simulations using real highway data. We showed that frequent updates of the status and intent information can further improve time efficiency and passenger comfort. Our future work include extending the framework using more detailed vehicle dynamics models, and implementing and validating intent-sharing messages on real vehicles.

APPENDIX I
PROOF OF LEMMA 1

($\Rightarrow$). The left hand side of (10) implies that for $(u_1, u_2) \equiv (a_{\min,1}, a_{\max,2})$, we have $\exists u_0, \exists t \geq 0, h_{10}(t) \geq s_{\mathrm{F}} \wedge h_{02}(t) \geq s_{\mathrm{R}}$. Thus, $h_{12}(t) = h_{10}(t) + h_{02}(t) + l \geq s_{\mathrm{F}} + s_{\mathrm{R}} + l$, implying that such t satisfies $t \in T$.

($\Leftarrow$). The right hand side of (10) implies that for $(u_1, u_2) \equiv (a_{\min,1}, a_{\max,2})$, we have $\exists u_0, P$. Let u_0^* and t^* denote an input u_0 and a time t such that $h_{10}(t^*) \geq$

$s_{\rm F} \wedge h_{02}(t^*) \geq s_{\rm R}$ under $(u_1, u_2) \equiv (a_{\min,1}, a_{\max,2})$. For $(u_1, u_2) \not\equiv (a_{\min,1}, a_{\max,2})$, the same input u_0^* leads to even larger h_{10} and h_{02} values at t^*, i.e., $h_{10}(t^*) \geq s_{\rm F} \wedge h_{02}(t^*) \geq s_{\rm R}$ still holds. Thus, $\forall u_1, \forall u_2, \exists u_0, P$.

Appendix II
Analytical form of $\delta(t)$, $h_{02}^{\min}(t)$, and $h_{02}^{\max}(t)$

Without intent information, we have $\delta(t) = r_1^*(t) - r_2^*(t) - s_{\rm F} - 2l$, where

$$r_1^*(t) = g(r_1(0), v_1(0), a_{\min,1}, v_{\min,1}, t), \tag{15}$$

$$r_2^*(t) = g(r_2(0), v_2(0), a_{\max,2}, v_{\max,2}, t), \tag{16}$$

$$g(r_2(0), v_2(0), a_{\max,2}, v_{\max,2}, t) = \tag{17}$$

$$\begin{cases} r_2(0) + v_2(0)t + \frac{1}{2}a_{\max,2}t^2 & \text{if } t \leq \frac{(v_{\max,2} - v_2(0))}{a_{\max,2}}, \\ r_2(0) - \frac{(v_{\max,2} - v_2(0))^2}{2a_{\max,2}} + v_{\max,2}t & \text{otherwise,} \end{cases}$$

and $h_{02}^{\min}(t) = r_0^*(t) - \underline{r}_2^*(t) - l$, $h_{02}^{\max}(t) = r_0^*(t) - \bar{r}_2^*(t) - l$, where

$$\underline{r}_0^*(t) = g(r_0(0), v_0(0), a_{\min,0}, v_{\min,0}, t), \tag{18}$$

$$\bar{r}_0^*(t) = g(r_0(0), v_0(0), a_{\max,0}, v_{\max,0}, t). \tag{19}$$

When intent information is available, $\delta(t)$, $h_{02}^{\min}(t)$, and $h_{02}^{\max}(t)$ can be calculated similarly using the equations above but with the following $r_1^*(t)$ and $r_2^*(t)$:

$$r_1^*(t) = \tag{20}$$

$$\begin{cases} g(r_1(0), v_1(0), \underline{a}_1, \underline{v}_1, t) & \text{if } t \leq \Delta t_1, \\ g(r_1^*(\Delta t_1), v_1^*(\Delta t_1), a_{\min,1}, v_{\min,1}, t - \Delta t_1) & \text{otherwise,} \end{cases}$$

$$r_2^*(t) = \tag{21}$$

$$\begin{cases} g(r_2(0), v_2(0), \bar{a}_2, \bar{v}_2, t) & \text{if } t \leq \Delta t_2, \\ g(r_2^*(\Delta t_2), v_2^*(\Delta t_2), a_{\max,2}, v_{\max,2}, t - \Delta t_2) & \text{otherwise,} \end{cases}$$

where $v_1^*(\Delta t_1) = \max(v_1(0) + \underline{a}_1 \Delta t_1, \underline{v}_1)$ and $v_2^*(\Delta t_2) = \min(v_2(0) + \bar{a}_2 \Delta t_2, \bar{v}_2)$.

Appendix III
Proof of Theorem 1

If $\Gamma \neq \emptyset$, then based on the definition of Γ in (11), under $(u_1, u_2) \equiv (a_{\min,1}, a_{\max,2})$, we have $\exists u_0, \exists t \in T, s_{\rm R} \leq h_{02}(t) \leq \delta(t)$. Substituting $\delta(t) = h_{12}(t) - s_{\rm F} - l$ yields $h_{02}(t) \leq h_{12}(t) - s_{\rm F} - l$, i.e., $s_{\rm F} \leq h_{10}(t)$. These and Lemma 1 imply $\mathbf{x}(0) \in \mathcal{P}_{\rm g}$.

If $\Gamma = \emptyset$, then under $(u_1, u_2) \equiv (a_{\min,1}, a_{\max,2})$, we have $\forall u_0(t), \forall t \in T, \neg\{s_{\rm R} \leq h_{02}(t) \leq \delta(t)\}$, i.e., $\neg\{h_{10}(t) \geq s_{\rm F} \wedge h_{02}(t) \geq s_{\rm R}\}$. Also, $\forall t \notin T$ we still have $\neg\{h_{10}(t) \geq s_{\rm F} \wedge h_{02}(t) \geq s_{\rm R}\}$. Thus, for $(u_1, u_2) \equiv (a_{\min,1}, a_{\max,2})$, $\forall u_0, \neg P$. This implies $\mathbf{x}(0) \notin \mathcal{P}_{\rm g}$.

Appendix IV
Controller $u_0^{\rm G}$

Given a goal point $(t^{\rm G}, h_{02}^{\rm G}) \in \Gamma$ (or $\bar{\Gamma}$), we have

$$u_0^{\rm G} = \begin{cases} \frac{2(s^{\rm G} - t^{\rm G} v_0)}{t^{\rm G\,2}}, & \text{if } s^{\rm G} \in [\frac{t^{\rm G}(v_0 + v_{\min,0})}{2}, \\ & \qquad \frac{t^{\rm G}(v_0 + v_{\max,0})}{2}], \\ f_1(v_0, t^{\rm G}, s^{\rm G}), & \text{if } s^{\rm G} \in [0, \frac{t^{\rm G}(v_0 + v_{\min,0})}{2}], \\ f_2(v_0, t^{\rm G}, s^{\rm G}), & \text{otherwise,} \end{cases} \tag{22}$$

where $s^{\rm G}$ is the distance that the ego vehicle must travel to secure rear gap $h_{02}^{\rm G}$ at $t^{\rm G}$ assuming the worst-case behavior of remote vehicle 2. That is, $s^{\rm G} = r_2^*(t^{\rm G}) - r_0(0) + h_{02}^{\rm G} + l$ for the $r_2^*(\cdot)$ given in Appendix II, and

$$f_1(v_0, t^{\rm G}, s^{\rm G}) = \begin{cases} \frac{2(s^{\rm G} - t^{\rm G} v_0)}{t^{\rm G\,2}}, & \text{if } a_{\min,0} \geq \frac{v_{\min,0} - v_0}{t^{\rm G}}, \\ \frac{(v_0 - v_{\min,0})^2}{2(t^{\rm G} v_{\min,0} - s^{\rm G})}, & \text{otherwise,} \end{cases} \tag{23}$$

$$f_2(v_0, t^{\rm G}, s^{\rm G}) = \begin{cases} \frac{2(s^{\rm G} - t^{\rm G} v_0)}{t^{\rm G\,2}}, & \text{if } a_{\max,0} \leq \frac{v_{\max,0} - v_0}{t^{\rm G}}, \\ \frac{(v_0 - v_{\max,0})^2}{2(t^{\rm G} v_{\max,0} - s^{\rm G})}, & \text{otherwise.} \end{cases} \tag{24}$$

Note that input $u_0^{\rm G}$ is divided into above different cases to take care of velocity saturation when traveling $s^{\rm G}$ within $t^{\rm G}$.

References

[1] SAE J3216, "Taxonomy and Definitions for Terms Related to Cooperative Driving Automation for On-Road Motor Vehicles," SAE International, Tech. Rep., 2021.

[2] C. Liu, C.-W. Lin, S. Shiraishi, and M. Tomizuka, "Distributed conflict resolution for connected autonomous vehicles," *IEEE Transactions on Intelligent Vehicles*, vol. 3, no. 1, pp. 18–29, 2020.

[3] M. R. Hafner, D. Cunningham, L. Caminiti, and D. Del Vecchio, "Cooperative collision avoidance at intersections: Algorithms and experiments," *IEEE Transactions on Intelligent Transportation Systems*, vol. 14, no. 3, pp. 1162–1175, 2013.

[4] J. Rios-Torres and A. A. Malikopoulos, "A survey on the coordination of connected and automated vehicles at intersections and merging at highway on-ramps," *IEEE Transactions on Intelligent Transportation Systems*, vol. 18, no. 5, pp. 1066–1077, 2016.

[5] SAE J3016, "Taxonomy and Definitions for Terms Related to Driving Automation Systems for On-Road Motor Vehicles," SAE International, Tech. Rep., 2021.

[6] B. M. Albaba and Y. Yildiz, "Modeling cyber-physical human systems via an interplay between reinforcement learning and game theory," *Annual Reviews in Control*, vol. 48, pp. 1–21, 2019.

[7] A. Bajcsy, S. L. Herbert, D. Fridovich-Keil, J. F. Fisac, S. Deglurkar, A. Dragan, and C. Tomlin, "A scalable framework for real-time multi-robot, multi-human collision avoidance," *2019 International Conference on Robotics and Automation (ICRA)*, pp. 936–943, 2019.

[8] M. Karimi, C. Roncoli, C. Alecsandru, and M. Papageorgiou, "Cooperative merging control via trajectory optimization in mixed vehicular traffic," *Transportation Research Part C: Emerging Technologies*, vol. 116, p. 102663, 2020.

[9] N. Williams, G. Wu, and M. Barth, "Position uncertainty-tolerant cooperative merging application for mixed multilane traffic," *IEEE Transactions on Intelligent Vehicles*, pp. 1–1, 2021.

[10] H. M. Wang, T. G. Molnár, S. S. Avedisov, A. H. Sakr, O. Altintas, and G. Orosz, "Conflict analysis for cooperative merging using v2x communication," in *2020 IEEE Intelligent Vehicles Symposium (IV)*, 2020, pp. 1538–1543.

[11] H. M. Wang, S. S. Avedisov, A. H. Sakr, O. Altintas, and G. Orosz, "Opportunistic strategy for cooperative maneuvering using conflict analysis," in *2021 IEEE Intelligent Vehicles Symposium (IV)*, 2021, pp. 348–353.

[12] H. M. Wang, S. S. Avedisov, T. G. Molnár, A. H. Sakr, O. Altintas, and G. Orosz, "Conflict analysis for cooperative maneuvering with status and intent sharing via v2x communication," *IEEE Transactions on Intelligent Vehicles*, 2022, doi: 10.1109/TIV.2022.3149796.

[13] SAE J2735, "Dedicated Short Range Communications (DSRC) Message Set Dictionary Set," SAE International, Tech. Rep., 2016.

[14] S. Haddad and A. Halder, "The convex geometry of integrator reach sets," in *2020 American Control Conference (ACC)*, 2020, pp. 4466–4471.

[15] N. Kochdumper and M. Althoff, "Sparse polynomial zonotopes: A novel set representation for reachability analysis," *IEEE Transactions on Automatic Control*, vol. 66, no. 9, pp. 4043–4058, 2021.